///VSP///

Advanced Composite Materials 18 (2009) 77–93

ADVANCED COMPOSITE MATERIALS
www.brill.nl/acm

Periodic-Cell Simulations for the Microscopic Damage and Strength Properties of Discontinuous Carbon Fiber-Reinforced Plastic Composites

M. Nishikawa [a,*], **T. Okabe** [b] **and N. Takeda** [c]

[a] Department of Aeronautics and Astronautics, The University of Tokyo, c/o Transdisciplinary Sciences Bldg. Mailbox 311, 5-1-5 Kashiwanoha, Kashiwa-shi, Chiba 277-8561, Japan

[b] Department of Aerospace Engineering, Tohoku University, 6-6-01 Aoba-yama, Aoba-ku, Sendai 980-8579, Japan

[c] Department of Advanced Energy, The University of Tokyo, c/o Transdisciplinary Sciences Bldg. Mailbox 302, 5-1-5 Kashiwanoha, Kashiwa-shi, Chiba 277-8561, Japan

Received 24 November 2008; accepted 29 November 2008

Abstract

This paper investigated the damage transition mechanism between the fiber-breaking mode and the fiber-avoiding crack mode when the fiber-length is reduced in the unidirectional discontinuous carbon fiber-reinforced-plastics (CFRP) composites. The critical fiber-length for the transition is a key parameter for the manufacturing of flexible and high-strength CFRP composites with thermoset resin, because below this limit, we cannot take full advantage of the superior strength properties of fibers. For this discussion, we presented a numerical model for the microscopic damage and fracture of unidirectional discontinuous fiber-reinforced plastics. The model addressed the microscopic damage generated in these composites; the matrix crack with continuum damage mechanics model and the fiber breakage with the Weibull model for fiber strengths. With this numerical model, the damage transition behavior was discussed when the fiber length was varied. The comparison revealed that the length of discontinuous fibers in composites influences the formation and growth of the cluster of fiber-end damage, which causes the damage mode transition. Since the composite strength is significantly reduced below the critical fiber-length for the transition to fiber-avoiding crack mode, we should understand the damage mode transition appropriately with the analysis on the cluster growth of fiber-end damage.

Keywords

Fiber-reinforced composite material, discontinuous fiber, microstructure, microscopic damage, strength, finite element method

* To whom correspondence should be addressed. Tel.: +81-4-7136-4031; Fax: +81-4-7136-4031; e-mail: nishikawa@smart.k.u-tokyo.ac.jp

Edited by JSCM

DOI:10.1163/156855108X399974

1. Introduction

Carbon fiber-reinforced plastics (CFRP) are currently being investigated for use as general industrial materials, such as in automobile applications. While continuous fiber-reinforced composites are frequently used for recent aerospace applications, in automobile applications, discontinuous fiber-reinforced composites have been increasingly applied to structural components because their flexibility is preferable to form into the complex-shaped structure. However, in general, CFRP made of short fibers suffers from severe matrix crack, which extends avoiding fibers (e.g., [1]), and then the matrix crack causes the fracture of the overall composite. To pursuit both the flexibility and high-strength of CFRP, it is necessary to discuss what length of the fiber is appropriate to take full advantage of the superior strength properties of the fiber. Thus we should understand how the dominant damage mode shifts from the fiber breakage in continuous CFRP to the fiber-avoiding matrix crack in discontinuous CFRP.

Various models have been proposed for the strength of discontinuous fiber-reinforced composite [2–4]. These models were simple extensions of the model used for continuous fiber-reinforced composites, taking into account initial random discontinuities inherent in discontinuous fiber-reinforced composites. The model given by Fukuda and Chou [3] paid special attention to the stress-concentration effect on the breakage of the neighboring fiber due to the discontinuities. The model given by Ibnabdeljalil and Phoenix [4] dealt with the statistical aspects of the strength of discontinuous fiber-reinforced composites, analyzing the fiber damage evolution along the fiber with initial discontinuities within a global load sharing (GLS) framework. Both models inherently assume that unless the fiber is fully covered by the stress-degraded region (ineffective length) around fiber breaks or fiber ends, the fiber breakage can occur and it causes the stress degradation of the composite. Thus the models yield the strength of the composites with considerably short fibers even when the fiber length is close to the ineffective length. However, these conventional approaches may not be correct. In realistic situations, the dominant damage process in composites shifts from the fiber damage evolution to the matrix crack propagation (Fig. 1) when the fiber length is reduced as described above.

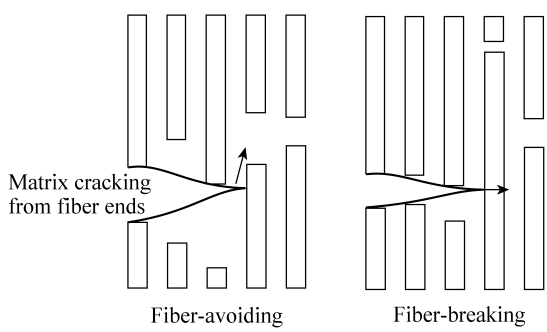

Figure 1. Damage process in discontinuous fiber-reinforced composites.

Therefore, the damage progress of the matrix crack from fiber ends has to be addressed with a detailed analysis, to understand the underlying damage mechanism of the strength degradation of discontinuous CFRP. The previous models are not sufficient for such a discussion.

This paper thoroughly discusses the damage transition mechanism between the fiber-breaking mode and the fiber-avoiding crack mode, which influences the strength of CFRP when the fiber length is reduced. The knowledge of the critical fiber length for the transition is essential to pursuit both the flexibility and high-strength of CFRP. The GLS models used for the strength of continuous CFRP have been extended to discuss the strength of discontinuous CFRP as described above, and these extended models are summarized in Section 2 as a comparison. However, these models cannot discuss the damage transition to the fiber-avoiding crack mode when the fiber length is reduced. Instead, Section 3 presents a numerical model for the fracture of unidirectional discontinuous CFRP, with consideration of matrix crack and fiber breakage. The model addresses the matrix crack with continuum damage mechanics model and the fiber breakage with the Weibull model for fiber strengths. Finally, Section 4 presents the simulated results and discusses the damage transition mechanisms between the fiber-avoiding and fiber-breaking modes.

2. Conventional Approach for Composite Strength

2.1. GLS Model

First of all, we discuss the strength of unidirectional discontinuous fiber-reinforced composites, based on GLS assumption [5, 6]. The GLS model focuses on one fragmented fiber (i.e., discontinuous fibers), aligned in the fiber axial direction, and neglect the interaction in the fiber cross-sectional direction between fibers. It predicts the composite's strength by simulating the fiber damage evolution in such a fiber. In simulating the fiber damage evolution for CFRP, we can utilize the Monte Carlo simulation with the elastic–plastic hardening shear-lag model given by Okabe and Takeda [7], because the fiber stress distribution in CFRP is mostly controlled by the matrix shear due to its superior interfacial properties [8, 9].

First, we will briefly explain the elastic–plastic shear-lag model. The axial length of the model was set to 100 mm, and the axial length was divided into 10 000 segments. The fiber ends in the discontinuous fiber-reinforced composites were represented by setting some random segments to the initially broken segments. Thus the averaged length of the discontinuous fibers was related to the density of the initially broken segments introduced in the model. The transverse length of matrix shear region in the model was set to $D = (\sqrt{2\pi/\sqrt{3}V_\mathrm{f}} - 2)r_\mathrm{f}$, as noted in Ref. [10]. (Here, r_f is the fiber radius, and V_f is the fiber volume fraction.) The plastic constitutive behavior of the matrix used linear-isotropic hardening function as

$$\bar{\sigma} = \sigma_\mathrm{y} + F_\mathrm{m}\bar{\varepsilon}^\mathrm{p}, \tag{1}$$

where $\bar{\sigma}$ is the effective stress, $\bar{\varepsilon}^{\mathrm{p}}$ is the equivalent plastic strain, σ_{y} is the matrix yield stress, and F_{m} is the matrix plastic modulus. With this model, we can calculate the fiber axial stress distribution of the unidirectionally aligned fiber at arbitrary applied strains with the elastic–plastic hardening shear-lag model.

Then this stress analysis was incorporated into Monte Carlo simulation technique to address the fiber damage evolution [11]. We first assigned the fiber strengths to initially unbroken segments based on Weibull model. In the Weibull model, the cumulative failure probability of a fiber segment of length Δ is given as

$$P_{\mathrm{f}}(\sigma) = 1 - \exp\left\{\left(-\frac{\Delta}{L_0}\right)\left(\frac{\sigma}{\sigma_0}\right)^{\rho'}\right\}, \tag{2}$$

where ρ' is Weibull modulus, and σ_0 is the characteristic strength of the fiber with length L_0. The actual strength σ_j for the jth fiber point was then chosen by selecting a random number R_j within (0, 1) and solving $R_j = P_{\mathrm{f}}(\sigma_j, \sigma_0)$. We judged the broken segments whose stress reaches the assigned strength with increasing applied strain. Thus we conducted the Monte Carlo simulation for the fiber damage evolution in unidirectional discontinuous fiber-reinforced composites.

The composite stress was determined by multiplying the fiber volume fraction and the fiber axial stress averaged for all segments. Thus the stress–strain relation of the composite could be obtained. The simulation terminated when the composite stress dropped to 90% of the maximum attained stress. The composite strength was then obtained as that maximum stress.

Throughout the paper, the simulations used the material properties for carbon fiber and epoxy matrix, listed in our previous literature [8]. The fiber volume fraction V_{f} was set to 40%. The fiber strength parameters were reported in our previous literature [7]. The Weibull scale parameter was $\sigma_0 = 4530$ MPa, gage length was $L_0 = 50$ mm, Weibull shape parameter was $\rho' = 15$.

2.2. Results and Discussion

Figure 2 presents the stress–strain relations and the density of fiber breaks as a function of the applied strain. The composite stress drops due to the accumulated fiber breaks. As the discontinuous fibers are short, the initial composite stiffness reduces because the stress-degraded region around fiber ends becomes large over the axial composite length. In contrast, the applied strain where fiber breaks begin to accumulate does not change so much when the fiber length is varied. This is because the breaking strain is solely controlled by the local fiber strength, when the fiber breakage occurs within the region where the fiber stress fully recovers to the far-field applied stress. That region may become small by the existence of fiber ends, but not small enough to influence the fiber breaking behavior. Therefore, according to the GLS predictions, the composite strength with a short fiber length reduces mostly due to the degradation of the stress-carrying capacity of the fiber accompanied with the increase of fiber ends.

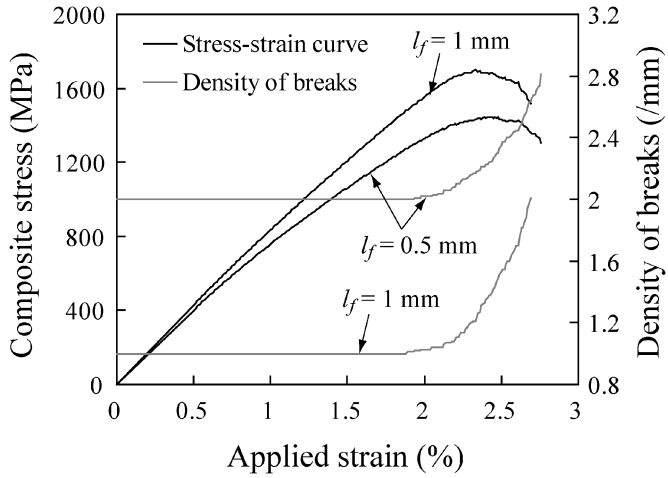

Figure 2. Fiber damage evolution and stress–strain curves predicted with GLS model.

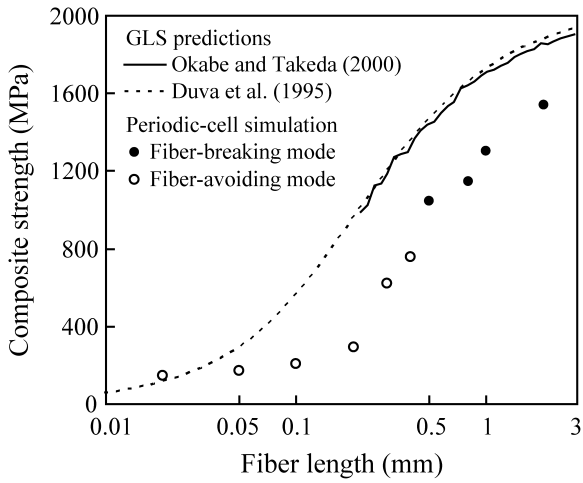

Figure 3. Comparison of the composite strength *versus* fiber length.

Figure 3 summarizes the composite strength obtained with the GLS model when the averaged fiber length is varied. The theoretical prediction based on Duva's GLS model [6] considering the fragmented length distribution of the fiber is also indicated in the figure. (This theoretical result was calculated through the incorporation of the fiber end effect into Duva's model by assuming an initial break density. Additionally, we substituted the result of the elastic–plastic hardening shear-lag model into the stress recovery length required in the calculation.) The tendency of the composite strength varying with fiber length is almost the same for both models. However, the result for the shorter fiber length is different. Duva's model permits fiber damage evolution regardless of the fiber length. In contrast, the Monte Carlo simulation reveals that the fiber breakage causing the critical degradation of the

composite stress does not occur in the case of the fiber length smaller than a certain critical length (219 μm). Thus we cannot define the composite strength in this range of fiber length. This situation is caused when the axial length of the fiber is fully covered by the stress-degraded region around fiber breaks or fiber ends. This critical fiber length characterizes the lower-limit length where the fiber breakage is the dominant damage in the final fracture of the composite. Below this limit, the final failure of the composite is not caused by the fiber breakage. It may be controlled by the matrix cracking process.

However, these theoretical models cannot address the stress-concentration effect of the matrix crack from fiber ends on neighboring fibers, nor the final failure caused by the fiber-avoidance crack. We will discuss these effects in the following sections.

3. Periodic-Cell Simulation for the Progressive Damage in Discontinuous CFRP

We next conducted periodic-cell simulations focusing on the extension of the matrix crack from fiber ends in discontinuous CFRP. As noted in the Introduction, the fundamental question to be discussed is how the fiber-avoiding and fiber-breaking damage modes occur. As pointed out by Xu *et al.* [12], when the fibers are strongly bonded to the surrounding material and the fiber is sufficiently strong, the crack is trapped by the fibers. Therefore, the damage mechanism after the matrix crack is trapped by the fibers (Fig. 1) is the most important to discuss. In the CFRP with short fibers, the matrix crack easily avoids the fibers and then advances. Thus the strength improvement by the fibers is limited. If the matrix crack cannot avoid the fibers, it cannot grow until the fiber breakage occurs ahead of it. This mechanism leads to the high strength of continuous CFRP. For this discussion, we simulated the interacting damage progress of fiber breakage and matrix crack within two-dimensional finite-element framework as below.

3.1. Periodic-Cell Model

Here we will briefly explain the periodic-cell model used in those simulations. The periodic-cell model assumes that the overall composite is composed of many unit-cell models aligned periodically. We employed the unit-cell models as illustrated in Fig. 4. We assumed a two-dimensional plane-strain condition. The unit-cell models contained randomly-arranged discontinuous fibers. The lengths of all fibers contained in the model are uniform. The number of fibers is determined so that the resulting volume fraction of fibers is accurate. The fiber volume fraction V_f was set to 40%. In this model, the fiber spacing locally reduces or increases due to the random arrangement of the fibers, and thus the matrix-rich region tends to become large in some regions.

The fibers consisted of nine-node quadrilateral elements and the matrix consisted of six-node triangle elements. It should be noted that the fiber width in the two-dimensional plane-strain model should be chosen as half the actual fiber diameter,

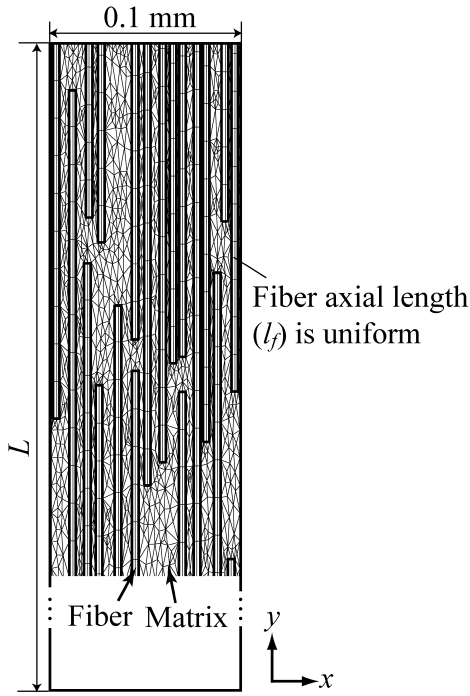

Figure 4. Unit-cell model for the periodic-cell simulation.

in order to reproduce the fiber axial stress distribution accurately [13]. The fiber was modeled as an orthotropic-elastic material while the matrix was assumed to be an isotropic elastic–plastic material. The plastic constitutive behavior of the matrix was based on J_2 flow theory and used linear-isotropic hardening function (1).

We analyzed the models with fiber length $l_f = 0.02$ mm, 0.05 mm, 0.1 mm, 0.2 mm, 0.3 mm, 0.4 mm, 0.5 mm, 0.8 mm, 1.0 mm, 2.0 mm. (The finite-element mesh shown in Fig. 4 is the part of the model with fiber length $l_f = 0.4$ mm.) The model length L in y-direction is adjusted to some extent for various fiber lengths. (Corresponding to each fiber length, we set $L = 0.525$ mm, 0.525 mm, 1.05 mm, 1.05 mm 1.47 mm, 1.47 mm, 2.1 mm, 2.1 mm, 2.1 mm, 2.1 mm.) All opposite sides of the unit cell were subject to periodic boundary conditions. As shown in Fig. 4, a fiber can be located on the periodic boundary in the unit-cell model. To enforce the periodicity condition, the nodes on one side of the unit-cell model were connected to those on the other side, so that both sides could deform equally. For this purpose, the same node number was assigned to each pair of corresponding nodes on opposite sides of the model.

3.2. Periodic-Cell Simulation

We next describe the simulation procedure to deal with the progressive damage (matrix crack and fiber breakage) in discontinuous CFRP.

3.2.1. Fiber Breakage

Our simulation considered the fiber breakage based on Weibull statistics. In the models, potential fiber break points were set in the direction perpendicular to the fiber axis with regular intervals. We set a large number of those paths for all fiber lengths, and the interval was sufficiently small (50 μm–100 μm) even in the case of the longest fibers. Fiber break was assumed to follow a maximum stress criterion with a Weibull statistical distribution of breaking strengths, described by (2), and we assigned the fiber strength at each potential break point. During the simulation, the fiber axial stress at the potential break points was monitored. When the fiber axial stress reached the critical stress given by the Weibull model, a fiber break was introduced by unloading the internal nodal force normal to the corresponding fiber-breaking surface.

3.2.2. Matrix Crack

We employed a one-parameter damage mechanics model to deal with the initiation and propagation of the matrix crack. As pointed out by, e.g., Fiedler *et al.* [14], the epoxy resin fails through the extension of existing defects due to normal stress followed by shear hackle failure. The damage mechanics model is useful to include these microscopic situations involved in the damage extension. For example, Kobayashi *et al.* [15] utilized the damage mechanics model to simulate the necking and failure process of ductile polymer at high applied strains. Here microscopic crazing evolution and annihilation could be reasonably incorporated into damage extension simulation of ductile polypropylene through the evolutionary equation of the damage variable. Therefore we extended this approach to epoxy fracture.

We begin with defining strain-equivalent configuration [16]. The variables in the nominal state (macroscopically homogenized state, or the state used in finite-element calculation) (stress σ, strain ε, stiffness E) can be expressed in relation to those in the true state (actual, microscopically damaged state) ($\sigma^*, \varepsilon^*, E_0$) as follows. (Here we write down one-dimensional description for simplicity.)

$$\varepsilon^* = \varepsilon, \qquad E = (1 - D)E_0 \to \sigma^* = \frac{\sigma}{1 - D}, \tag{3}$$

where D denotes the damage variable causing the stiffness degradation. As D increases, the stiffness reduces till finally $E = 0$ when $D = 1$. For the elastic–plastic matrix, the multi-dimensional incremental stress–strain relations can be derived as below.

$$\Delta\boldsymbol{\sigma} = (1 - D)\mathbf{C}^{\mathrm{ep}} : \Delta\boldsymbol{\varepsilon} - \frac{\Delta D}{1 - D}\boldsymbol{\sigma}, \tag{4}$$

where $\mathbf{C}^{\mathrm{ep}}$ is the elastic–plastic constitutive tensor. Here the damage variable is defined as scalar quantity.

The microscopic failure characteristics can be incorporated into the evolutionary equation of damage variable. Here we define the following evolutionary equation

of damage variable.

$$\Delta D = (1 - D)C\langle \Delta\varepsilon_{\mathrm{m}}^{\mathrm{p}} \rangle + (B_0 + B_1 D)\Delta\bar{\varepsilon}^{\mathrm{p}} \quad (0 \leqslant D \leqslant 1), \tag{5}$$

$$\text{where } C\Delta\varepsilon_{\mathrm{m}}^{\mathrm{p}} = A\Delta\left\{ D\left(\frac{\langle \sigma_{\mathrm{m}} \rangle}{\sigma_{\mathrm{y}}} \right)^2 \right\}.$$

The first term represents the extension of existing voids or defects due to plastic volumetric expansion strain $\varepsilon_{\mathrm{m}}^{\mathrm{p}}$ (referring to Gurson's famous equation [17]), while the second term represents the damage extension due to shear failure. $\bar{\varepsilon}^{\mathrm{p}}$ denotes the plastic equivalent strain and σ_{m} denotes the mean stress. The meaning of the bracket $\langle\,\rangle$ in (5) is $\langle X \rangle = X$ $(X \geqslant 0)$, 0 $(X < 0)$. As D increases, the contribution of the first term reduces, which means that the void growth is suppressed by neighboring voids, and then the shear failure dominates. This reflects the microscopic situations in epoxy fracture. The similar treatment for the first term can be found in the literature by Kobayashi *et al.* (Here we simplified the definition of the volumetric expansion strain increment by parabolic fitting, referring to their preliminary FEM results.) The phenomelogical parameters in (5) are A, B_0 and B_1. We further simplified $B_0 = 0$ in this study. Here it is noted that the damage variable does not increase without setting the initial value of D (physically initial defects) in the case of $B_0 = 0$. Therefore, we set the initial value of D denoted by D_{ini} to a small value.

Matrix crack was judged at the integration point of each finite-element. When D approached 1, the contribution to the stiffness matrix became near zero and sometimes numerical instability occurred. Therefore, we eliminated the corresponding element when the averaged D in the element reached D_{cr} (near 1). The successive elimination process yielded free nodes. We searched for such nodes and excluded them from the equilibrium equations of the finite-element analysis. By this procedure, we simulated the initiation and propagation of matrix crack.

In Ref. [13], we applied this model to simulate the microscopic damage in single-fiber composite (SFC) tests using carbon-fiber and epoxy-matrix system. We demonstrated that the matrix crack model could reasonably reproduce the characteristic transverse matrix crack from a fiber break in the tests. Then the phenomelogical parameters A, B_0 and B_1 in (5) were reasonably calibrated through the comparison with SFC test results. Then we used the calibrated parameters $A = 0.5$, $B_0 = 0$, $B_1 = 0.5$ and $D_{\mathrm{ini}} = 0.01$ as the initial value of D. In addition, we used the same matrix crack model for interpreting the microscopic experimental phenomena in Ref. [18].

3.2.3. Finite-Element Formulation

Finally, we present the finite-element formulation of the present simulation. The virtual work for the analytical region with fiber region V_{f} and matrix region V_{m} is as follows:

$$\int_{V_{\mathrm{f}}} \boldsymbol{\sigma} : \delta\boldsymbol{\varepsilon}\,\mathrm{d}V + \int_{V_{\mathrm{m}}} \boldsymbol{\sigma} : \delta\boldsymbol{\varepsilon}\,\mathrm{d}V = \int_{S_{\mathrm{t}}} \mathbf{f} \cdot \delta\mathbf{u}\,\mathrm{d}S. \tag{6}$$

Here, $\boldsymbol{\sigma}$ is the stress tensor, $\boldsymbol{\varepsilon}$ is the strain tensor, $\mathbf{u}$ is the displacement vector, $\mathbf{f}$ is the external force vector on the prescribed boundary S_{t} and δ is the virtual component.

We consider a quasistatic rate formulation by expanding the virtual work equation at time $t' = t + \Delta t$ around the (assumed known) state prevailing at time t to linear order in Δt as

$$\Delta t\left(\int_{V_\mathrm{f}} {}^t\dot{\boldsymbol{\sigma}} : \delta\boldsymbol{\varepsilon}\,\mathrm{d}V + \int_{V_\mathrm{m}} {}^t\dot{\boldsymbol{\sigma}} : \delta\boldsymbol{\varepsilon}\,\mathrm{d}V\right) = \int_{S_\mathrm{t}} {}^{t'}\mathbf{f}\cdot\delta\mathbf{u}\,\mathrm{d}S - \left(\int_{V_\mathrm{f}} {}^t\boldsymbol{\sigma} : \delta\boldsymbol{\varepsilon}\,\mathrm{d}V + \int_{V_\mathrm{m}} {}^t\boldsymbol{\sigma} : \delta\boldsymbol{\varepsilon}\,\mathrm{d}V\right), \tag{7}$$

where $\dot{}$ denotes the time derivative.

In (7), the constitution law of solid elements is given by

$$\begin{aligned} \dot{\boldsymbol{\sigma}} &= \mathbf{C}_\mathrm{f}^\mathrm{e} : \dot{\boldsymbol{\varepsilon}} && \text{for fiber,} \\ \dot{\boldsymbol{\sigma}} &= (1-D)\mathbf{C}_\mathrm{m}^\mathrm{ep} : \dot{\boldsymbol{\varepsilon}} - \frac{\dot{D}}{1-D}\boldsymbol{\sigma} && \text{for matrix,} \end{aligned} \tag{8}$$

where $\mathbf{C}$ is the fourth-order tensor of the constitution law, subscripts f and m denote fiber and matrix, respectively, and superscripts e and ep denote elastic and elastic–plastic materials, respectively. The effect of matrix cracking and plasticity is implemented through this constitutive law of matrix. Then, equation (7) is transformed into the following equation:

$$\int_{V_\mathrm{f}} (\mathbf{C}_\mathrm{f}^\mathrm{e} : \Delta\boldsymbol{\varepsilon}) : \delta\boldsymbol{\varepsilon}\,\mathrm{d}V + \int_{V_\mathrm{m}} \big((1-D)\mathbf{C}_\mathrm{m}^\mathrm{ep} : \Delta\boldsymbol{\varepsilon}\big) : \delta\boldsymbol{\varepsilon}\,\mathrm{d}V = \int_{S_\mathrm{t}} {}^{t'}\mathbf{f}\cdot\delta\mathbf{u}\,\mathrm{d}S - \int_{V_\mathrm{f}+V_\mathrm{m}} {}^t\boldsymbol{\sigma} : \delta\boldsymbol{\varepsilon}\,\mathrm{d}V + \int_{V_\mathrm{m}} \frac{\Delta D}{1-D}({}^t\boldsymbol{\sigma} : \delta\boldsymbol{\varepsilon})\,\mathrm{d}V. \tag{9}$$

Now this formulation was coupled with a periodic-cell simulation technique (e.g., [19]) to conduct simulations using the periodic-cell model. Following the routine operation employed in the homogenization technique (e.g., [20]), let us first separate the displacement $\mathbf{u}$ and strain increment $\Delta\boldsymbol{\varepsilon}$ into global components, which are independent of the coordinates in the unit cell model, and local components as follows.

$$\mathbf{u} = \mathbf{u}_\mathrm{G} + \mathbf{u}_\mathrm{L} \quad \text{and} \quad \Delta\boldsymbol{\varepsilon} = \Delta\boldsymbol{\varepsilon}_\mathrm{G} + \Delta\boldsymbol{\varepsilon}_\mathrm{L}, \tag{10}$$

where subscripts G and L denote the global and local components, respectively. By these decompositions into global and local components, the basic incremental equation for virtual work (equation (9)) is transformed into the following equation for the unit-cell model with periodic boundaries.

$$\begin{aligned} &\int_{V_\mathrm{f}} (\mathbf{C}_\mathrm{f}^\mathrm{e} : \Delta\boldsymbol{\varepsilon}_\mathrm{L}) : \delta\boldsymbol{\varepsilon}\,\mathrm{d}V + \int_{V_\mathrm{m}} \big((1-D)\mathbf{C}_\mathrm{m}^\mathrm{ep} : \Delta\boldsymbol{\varepsilon}_\mathrm{L}\big) : \delta\boldsymbol{\varepsilon}\,\mathrm{d}V \\ &\quad = -\int_{V_\mathrm{f}+V_\mathrm{m}} {}^t\boldsymbol{\sigma} : \delta\boldsymbol{\varepsilon}\,\mathrm{d}V + \int_{V_\mathrm{m}} \frac{\Delta D}{1-D}({}^t\boldsymbol{\sigma} : \delta\boldsymbol{\varepsilon})\,\mathrm{d}V \\ &\qquad - \int_{V_\mathrm{f}} (\mathbf{C}_\mathrm{f}^\mathrm{e} : \Delta\boldsymbol{\varepsilon}_\mathrm{G}) : \delta\boldsymbol{\varepsilon}\,\mathrm{d}V - \int_{V_\mathrm{m}} \big((1-D)\mathbf{C}_\mathrm{m}^\mathrm{ep} : \Delta\boldsymbol{\varepsilon}_\mathrm{G}\big) : \delta\boldsymbol{\varepsilon}\,\mathrm{d}V, \end{aligned} \tag{11}$$

where the traction boundary S_t as in (9) does not exist in the present periodic-cell simulation. The global strain increment $\Delta\boldsymbol{\varepsilon}_G$ should be controlled to achieve loading conditions in the periodic cell.

Finally, the discretized form of (11) is the matrix equation as follows:

$$({}^t\mathbf{K}_f + {}^t\mathbf{K}_m)\Delta\mathbf{U}_L = -({}^t\mathbf{Q}_f + {}^t\mathbf{Q}_m) + {}^t\mathbf{Q}_{dam} - (\Delta\mathbf{Q}_{f,G} + \Delta\mathbf{Q}_{m,G}), \tag{12}$$

where:

$$\begin{aligned}
\mathbf{K}_f &= \sum_e \int_{V_f^e} \mathbf{B}^{e^T}\mathbf{D}_f^e\mathbf{B}^e \,\mathrm{d}V,\\
\mathbf{K}_m &= \sum_e \int_{V_m^e} (1-D)\mathbf{B}^{e^T}\mathbf{D}_m^{ep}\mathbf{B}^e \,\mathrm{d}V,\\
\mathbf{Q}_f &= \sum_e \int_{V_f^e} \mathbf{B}^{e^T}\hat{\boldsymbol{\sigma}} \,\mathrm{d}V,\\
\mathbf{Q}_m &= \sum_e \int_{V_m^e} \mathbf{B}^{e^T}\hat{\boldsymbol{\sigma}} \,\mathrm{d}V,\\
\mathbf{Q}_{dam} &= \sum_e \int_{V_m^e} \frac{\Delta D}{1-D}\mathbf{B}^{e^T}\hat{\boldsymbol{\sigma}} \,\mathrm{d}V,\\
\Delta\mathbf{Q}_{f,G} &= \sum_e \int_{V_f^e} \mathbf{B}^{e^T}\mathbf{D}_f^e\Delta\boldsymbol{\varepsilon}_G \,\mathrm{d}V,\\
\Delta\mathbf{Q}_{m,G} &= \sum_e \int_{V_m^e} (1-D)\mathbf{B}^{e^T}\mathbf{D}_m^{ep}\Delta\boldsymbol{\varepsilon}_G \,\mathrm{d}V,
\end{aligned} \tag{13}$$

where $\mathbf{U}$ is the nodal displacement vector, $\mathbf{K}_f$ and $\mathbf{K}_m$ are the tangential stiffness matrices of fiber and matrix elements, $\mathbf{Q}_f$ and $\mathbf{Q}_m$ are the nodal forces corresponding to the element stresses. $\mathbf{B}$ is the strain–displacement matrix, $\mathbf{D}$ is the constitutive matrix, and $\mathbf{F}$ is the externally applied nodal forces. The effect of constitution law for the matrix (equation (8)) is included in the expression in the matrix stiffness $\mathbf{K}_m$ and the added nodal force $\mathbf{Q}_{dam}$. $\Delta\mathbf{Q}_{f,G}$ and $\Delta\mathbf{Q}_{m,G}$ are the contributions by the predetermined global strain increment $\Delta\boldsymbol{\varepsilon}_G$. Equation (12) is the basic equation for the present periodic-cell simulation.

The periodic-cell simulations could be conducted by controlling the global strain increment $\Delta\boldsymbol{\varepsilon}_G$. In an incremental step in the simulation, we first calculated the displacement increment $\Delta\mathbf{U}_L$ by solving equation (12) under periodic boundary conditions. The total strain increment $\Delta\boldsymbol{\varepsilon}$ was calculated by adding the predetermined $\Delta\boldsymbol{\varepsilon}_G$ to $\Delta\boldsymbol{\varepsilon}_L$. Then the stress $\boldsymbol{\sigma}$ in the unit cell could be obtained with equation (8).

4. Simulated Results and Discussion

We present the results of the periodic-cell simulation for the progressive damage in discontinuous CFRP under a tensile load. The simulations were conducted

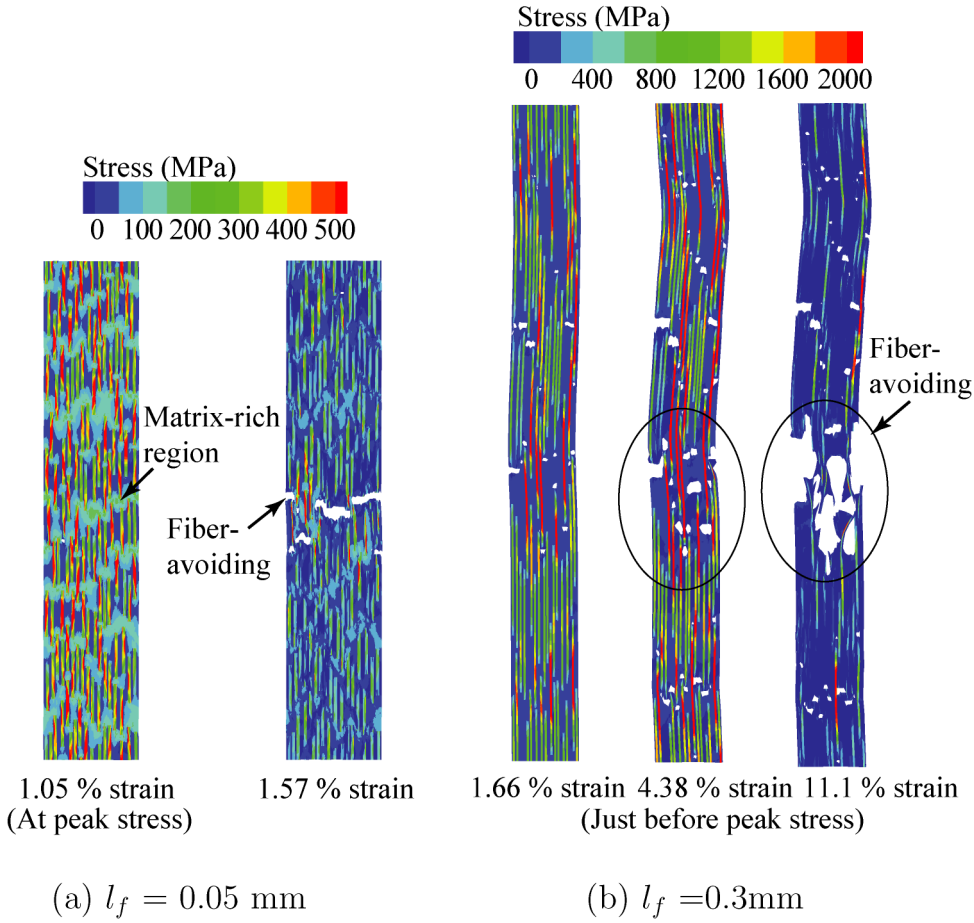

Figure 5. Comparison of the simulated damage when the fiber length l_f is varied. This figure is published in color on http://www.ingentaconnect.com/content/vsp/acm

by controlling strain increment proportionally ($\Delta\boldsymbol{\varepsilon}_G = (\Delta\varepsilon_{xx}, \Delta\varepsilon_{yy}, \Delta\varepsilon_{xy})_G = \alpha(-0.3, 1.0, 0.0)$), considering the Poisson's effect approximately. The composite stress is defined as the average of the normal stress σ_{yy} in y-direction all over the unit cell. The simulations used the same material properties and fiber strength parameters (equation (2)) as those used in Section 2. Other parameters for matrix crack (equation (5)) were described in Section 3.2. The simulations were conducted with Intel(R) Visual Fortran Compiler 9.0 on a Windows XP computer. We used PARDISO Direct Sparse Solver provided in Intel(R) Math Kernel Library 8.0 as a solver.

Figure 5 presents the simulated results. The stress in the figure is the normal stress in y-direction. (It should be noted that the deformation plot was generated by considering the local displacement $\mathbf{u}_L$ only. For this reason, the damage in the figure appears to have a large opening displacement.) The tensile stress–strain relations

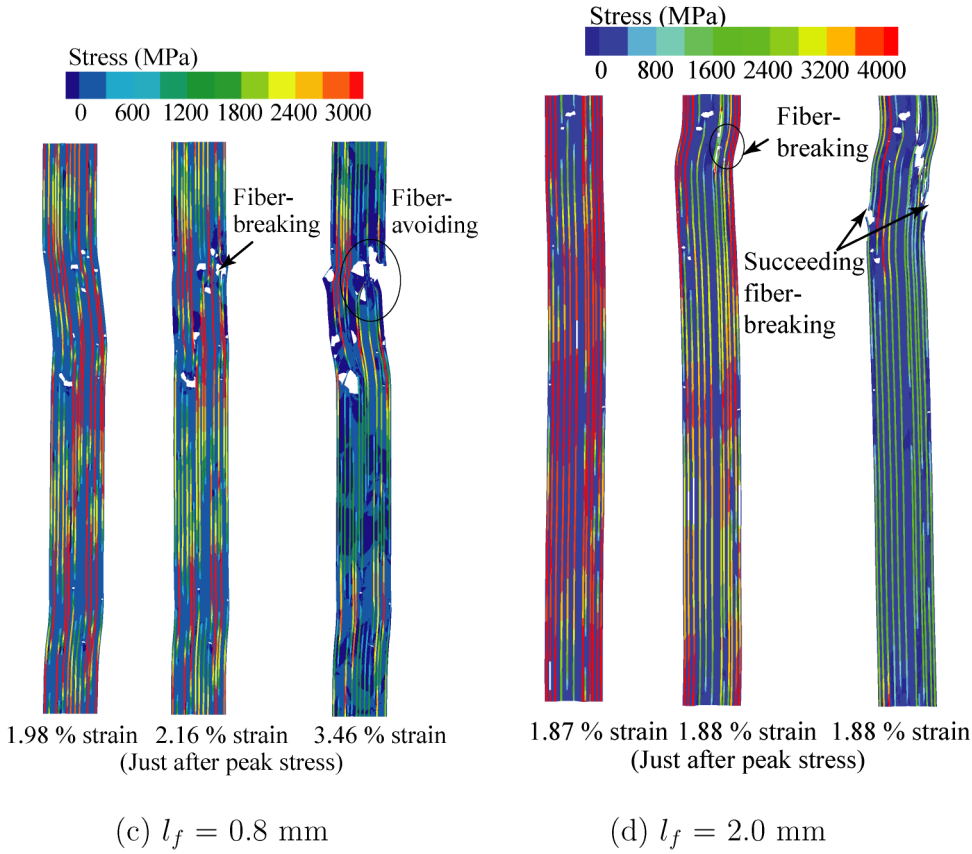

Figure 5. (Continued.)

of the composites obtained with those simulations are presented in Fig. 6. Below we discuss the relation between this microscopic damage process and macroscopic stress–strain response, referring to these figures.

First, when the fiber length is very small ($l_f = 0.05$ mm), the matrix crack accumulates at multiple fiber ends, and it propagates as it avoids the neighboring fiber (Fig. 5(a)). These matrix cracks tend to accumulate and propagate more readily in the matrix-rich region. In this range of short fiber lengths, the composite stress is reduced instantaneously after the initiation of multiple fiber end damage, as shown in Fig. 6. Thus the peak stress of the composite is controlled by that initiation.

When the fiber length increases, as found in Fig. 5(b) ($l_f = 0.3$ mm), the cluster of the accumulated fiber end damage stops extending as it is trapped by the fiber in the advancing direction (i.e., x-direction). In this case, as seen in Fig. 6, even after the composite stress drops due to the formation of the cluster of matrix crack, it resumes increasing since the stress is carried by the fibers that trap that cluster. At a high applied strain, the matrix crack avoids those trapping fibers and coalesces by causing the shear fracture of the matrix between fibers, as seen in Fig. 5(b). Then the

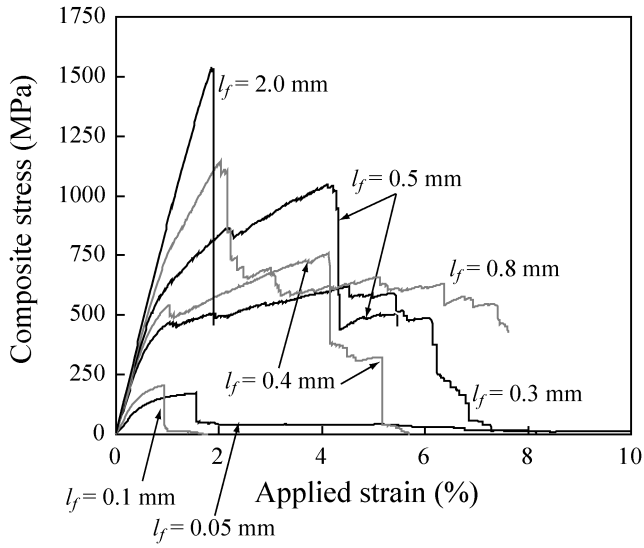

Figure 6. Simulated stress–strain curves when the fiber length l_f is varied.

stress carried by fibers is significantly reduced, which causes, as a consequence, the critical stress degradation of the composite. Therefore, the fracture of the composite with this fiber length range is still characterized by the fiber-avoiding mode of the matrix crack.

As the fiber length further increases, the cluster of matrix crack cannot propagate in a fiber-avoiding mode, as found in Fig. 5(c) ($l_f = 0.8$ mm). Instead, the cluster of matrix crack finally grows with the breakage of the trapping fibers. This fiber breakage leads to the reduction of the composite stress (Fig. 6). In the cases of even longer fibers, the composite fracture is characterized by the fiber-breaking mode. For long fibers (Fig. 5(d) ($l_f = 2.0$ mm)), the cluster further grows with successive fiber breakages according to the state of local fiber-strength variability and stress concentration, which is similar to the damage mode in continuous fiber-reinforced composites. Then the composite stress reduces drastically just after the maximum stress.

Finally, Fig. 3 plotted the composite strength, defined as the maximum stress in stress–strain curves, as a function of the fiber length l_f. In the figure, the hollow symbol indicates the cases where the peak stress is controlled by the fiber-avoiding mode, while the filled symbol indicates the cases of the fiber-breaking mode. The propagation mode is selectively determined by the fiber length, and the critical length for the transition between fiber-breaking and fiber-avoiding modes lies between 0.4 mm and 0.5 mm. When the reinforcing fiber becomes shorter than this critical length, the composite strength terribly reduces, as the matrix crack is likely to propagate in a fiber-avoiding mode. A high strength level of the composite can be maintained in the cases of fiber-breaking modes for the long fiber length.

The results with the GLS model described in Section 2 were also plotted in Fig. 3. It is found that the critical fiber length predicted with periodic-cell simulations is larger than the GLS prediction (219 μm). This implies that the GLS prediction cannot be correct. For example, for $l_f = 0.3$ mm (Fig. 5(b)), the cluster of matrix crack does not yield a sufficient stress concentration on nearby fibers, and then the fiber-avoiding coalescence is selectively caused. Then the critical fiber length is very sensitive to local factors; the stress-concentration effect of the cluster on nearby fibers to influence the fiber breakage, and the distance between fiber ends to influence the fiber-avoiding propagation. This situation is completely different from that assumed in the GLS model. Therefore, the critical length predicted with the GLS model is not appropriate to judge whether we can take full advantage of the superior strength properties of the fiber, because the strength is significantly reduced for the composite with that length.

In summary, the composite strength for the fiber length near the transition-length is influenced by quite complicated factors; the stress-concentration effect of the fiber end damage cluster, and the selective cluster growth in a fiber-avoiding or fiber-breaking mode according to the stress field. The mechanism assumed in Ref. [2, 3] for the strength of discontinuous fiber-reinforced composites was rather analogous to that discussed above in that the stress-concentration effect of the fiber end damage cluster was included. However, their model only predicted the susceptibility to fiber breakage due to the stress concentration of the cluster, and it could not address the statistics of fiber breakage nor the cluster growth itself. Only within the range of very long fiber lengths, the matrix crack cannot propagate at all, and then the composite strength can be discussed by simulating the fiber damage evolution including the stress-concentration effect of fiber end damage. This situation is quite similar to that assumed generally in local load-sharing (LLS) models, and for example, the simulation for the fiber damage evolution in our literatures [10, 21] is useful to discuss the strength of discontinuous fiber-reinforced composites within this range of fiber length.

Moreover, we can conclude that the cluster of fiber ends and/or locally large matrix-rich region have significant effects on the composite strength, when we use the fiber length near the critical fiber length. If an improved material design makes it possible to adjust the fiber alignment so that the clusters of fiber ends and matrix-rich regions are reduced, then we can shift the transition length to shorter fiber length to explore the maximized flexibility of CFRP without degradation of the strength.

5. Conclusions

This paper investigated the damage transition mechanism between the fiber-breaking mode and the fiber-avoiding crack mode when the fiber length is reduced, which influences the strength of CFRP. The critical fiber length for the transition is a key parameter for the manufacturing of flexible and high-strength CFRP com-

posites with thermoset resin. For this discussion, we presented a numerical model to address the matrix crack with continuum damage mechanics model and the fiber breakage with the Weibull model for fiber strengths. With this numerical model, the damage transition behavior was discussed.

For the unidirectional discontinuous CFRP, the damage mode causing the final fracture is divided into two patterns; the fiber-breaking and fiber-avoiding modes when the matrix crack from fiber ends propagates. The transition between fiber-breaking and fiber-avoiding modes occurs when the length of discontinuous fibers is varied. The composite strength significantly reduces around the critical fiber length for the damage-mode transition as the fiber length is reduced. A high strength level of the composite can be maintained only in the cases of fiber-breaking modes for the long fiber length. Therefore, we should identify the critical length for the transition appropriately to discuss the strength degradation of discontinuous CFRP when the fiber length is reduced.

The critical fiber length for the transition was also obtained with periodic-cell simulations. The length was longer than the critical length predicted with GLS model. This is because the critical fiber length is very sensitive to local factors; the stress-concentration effect of the cluster on nearby fibers to influence the fiber breakage, and the distance between fiber ends to influence the fiber-avoiding propagation, which are not considered in GLS models. Basically, the mechanisms assumed by the previous models were only one aspect of the composite fracture. In contrast, we have got a clear picture of the composite fracture, using the simulations dealing with both fiber breakage and matrix crack. The composite fracture is closely related to several mechanisms involving the cluster formation, stress concentration of the cluster, the selection of fiber-breaking or fiber-avoiding mode, the cluster growth and fracture. This is the most important conclusion of our paper.

Acknowledgement

T. O. acknowledges the New Energy and Industrial Technology Development Organization (NEDO) (Project No. P08024) for support.

References

1. J. F. Mandell, D. D. Huang and F. J. McGarry, Crack propagation modes in injection molded fiber reinforced thermoplastics, in: *Short Fiber Reinforced Composite Materials*, ASTM STP772, B. A. Sanders (Ed.), pp. 3–32. American Society for Testing and Materials (1982).
2. H. Fukuda and T. W. Chou, A probabilistic theory for the strength of short fibre composites, *J. Mater. Sci.* **16**, 1088–1096 (1981).
3. H. Fukuda and T. W. Chou, A probabilistic theory of the strength of short-fibre composites with variable fibre length and orientation, *J. Mater. Sci.* **17**, 1003–1011 (1982).
4. M. Ibnabdeljalil and S. L. Phoenix, Scalings in the statistical failure of brittle matrix composites with discontinuous fibers — I. Analysis and Monte Carlo simulations, *Acta Metallurgica et Materialia* **43**, 2975–2983 (1995).

5. J. M. Numeister, A constitutive law for continuous fiber reinforced brittle matrix composites with fiber fragmentation and stress recovery, *J. Mech. Phys. Solid.* **41**, 1383–1404 (1993).
6. J. M. Duva, W. A. Curtin and H. N. G. Wadley, An ultimate tensile strength dependence on processing for consolidated metal matrix composites, *Acta Metall. Mater.* **43**, 1119–1126 (1995).
7. T. Okabe and N. Takeda, Elastoplastic shear-lag analysis of single-fiber composites and strength prediction of unidirectional multi-fiber composites, *Composites A* **33**, 1327–1335 (2002).
8. M. Nishikawa, T. Okabe and N. Takeda, Determination of interface properties from experiments on the fragmentation process in single-fiber composites, *Mater. Sci. Eng. A* **480**, 549–557 (2008).
9. M. Nishikawa, T. Okabe, N. Takeda and W. A. Curtin, Micromechanics of the fragmentation process in single-fiber composites, *Model. Simulat. Mater. Sci. Eng.* **16**, 055009 (2008).
10. T. Okabe, M. Nishikawa, N. Takeda and H. Sekine, Effect of matrix hardening on tensile strength of alumina-fiber reinforced aluminum matrix composites, *Acta Mater.* **54**, 2557–2566 (2006).
11. T. Okabe and N. Takeda, Estimation of strength distribution for a fiber embedded in a single-fiber composite: experiments and statistical simulation based on the elastic–plastic shear-lag approach, *Compos. Sci. Technol.* **61**, 1789–1800 (2001).
12. G. Xu, A. F. Bower and M. Ortiz, The influence of crack trapping on the toughness of fiber reinforced composites, *J. Mech. Phys. Solid.* **46**, 1815–1833 (1998).
13. M. Nishikawa, Multiscale modeling for the microscopic damage and fracture of fiber-reinforced plastic composites, *Doctor Thesis*, Department of Aeronautics and Astronautics, The University of Tokyo (2008) (in Japanese).
14. B. Fiedler, M. Hojo, S. Ochiai, K. Schulte and M. Ando, Failure behavior of an epoxy matrix under different kinds of static loading, *Compos. Sci. Technol.* **61**, 1615–1624 (2001).
15. S. Kobayashi, D. Tomii and K. Shizawa, A modelling and simulation on failure prediction of ductile polymer based on craze evolution and annihilation, *Trans. Jpn. Soc. Mech. Eng. A* **70**, 810–817 (2004) (in Japanese).
16. S. Murakami and N. Ohno, A continuum theory of creep and creep damage, in: *Creep in Structures*, A. R. S. Ponter and D. R. Hyhurs (Eds), pp. 422–444. Springer-Verlag (1981).
17. A. L. Gurson, Continuum theory of ductile rupture by void nucleation and growth: Part I — Yield criteria and flow rules for porous ductile media, *Trans. ASME — J. Eng. Mater. Technol.* **99**, 2–15 (1977).
18. M. Nishikawa, T. Okabe, K. Hemmi and N. Takeda, Micromechanical modeling of the microbond test to quantify the interfacial properties in fiber-reinforced composites, *Int. J. Solid Struct.* **45**, 4098–4113 (2008).
19. K. Matous and P. H. Geubelle, Multiscale modeling of particle debonding in reinforced elastomers subjected to finite deformations, *Int. J. Numer. Meth. Eng.* **65**, 190–223 (2006).
20. N. Ohno, D. Okumura and H. Noguchi, Microscopic symmetric bifurcation analysis for cellular solids based on a homogenization theory of finite deformation (1st report, theory), *Trans. Jpn. Soc. Mech. Eng. A* **67**, 618–624 (2001) (in Japanese).
21. T. Okabe, H. Sekine, K. Ishii, M. Nishikawa and N. Takeda, Numerical method for failure simulation of unidirectional fiber-reinforced composites with spring element model, *Compos. Sci. Technol.* **65**, 921–933 (2005).